1   # Historical atmospheric pollution trends in Southeast Asia inferred from lake

2   # sediment records

3

4   Engels S[1,2*], Fong LSRZ[3], Chen Q[3], Leng MJ[1,4], McGowan S[1,5], Idris M[6], Rose NL[7], Shafiq M[6], Taylor D[3],

5   Yang H[7]

6

7   Affiliations
8   [1] Centre for Environmental Geochemistry, School of Geography, University of Nottingham,
9   Nottingham, NG7 2RD, UK
10   [2] School of Geography, Birkbeck University of London, Malet Street, London, WC1E 7HX, UK
11   [3] Department of Geography, National University of Singapore, Singapore, 117570, Singapore
12   [4] NERC Isotope Geosciences Facilities, British Geological Survey, Nottingham, NG12 5GG, UK
13   [5] School of Environmental and Geographical Sciences, University of Nottingham-Malaysia Campus,
14   Jalan Broga, 43500 Semenyih, Selangor Darul Ehsan, Malaysia
15   [6] Tasik Chini Research Centre, Faculty of Science and Technology, Universiti Kebangsaan Malaysia,
16   43600, Malaysia
17   [7] Environmental Change Research Centre, Department of Geography, University College London,
18   London, WC1E 6BT, UK
19   [*] author for correspondence; s.engels@bbk.ac.uk

20 **Abstract**

21 Fossil fuel combustion leads to increased levels of air pollution, which negatively affects human

22 health as well as the environment. Documented data for Southeast Asia (SEA) show a strong

23 increase in fossil fuel consumption since 1980, but information on coal and oil combustion before

24 1980 is not widely available. Spheroidal carbonaceous particles (SCPs) and heavy metals, such as

25 mercury (Hg), are emitted as by-products of fossil fuel combustion and may accumulate in sediments

26 following atmospheric fallout. Here we use sediment SCP and Hg records from several freshwater

27 lentic ecosystems in SEA (Malaysia, Philippines, Singapore) to reconstruct long-term, region-wide

28 variations in levels of these two key atmospheric pollution indicators. The age-depth models of

29 Philippine sediment cores do not reach back far enough to date first SCP presence, but single SCP

30 occurrences are first observed between 1925 and 1950 for a Malaysian site. Increasing SCP flux is

31 observed at our sites from 1960 onward, although individual sites show minor differences in trends.

32 SCP fluxes show a general decline after 2000 at each of our study sites. While the records show

33 broadly similar temporal trends across SEA, absolute SCP fluxes differ between sites, with a record

34 from Malaysia showing SCP fluxes that are two orders of magnitude lower than records from the

35 Philippines. Similar trends in records from China and Japan represent the emergence of atmospheric

36 pollution as a broadly-based inter-region environmental problem during the 20th century. Hg fluxes

37 were relatively stable from the second half of the 20th century onward. As catchment soils are also

38 contaminated with atmospheric Hg, future soil erosion can be expected to lead to enhanced Hg flux

39 into surface waters.

40

41 'Capsule' – Lake sediment records from Southeast Asia provide first data on historical trends in

42 fossil-fuel derived atmospheric pollution

43

44 Keywords: fossil fuel combustion; emission trends; fly ash particles; mercury; Southeast Asia

45

46 Highlights

47 - First data on historical atmospheric pollution trends in Southeast Asia

48 - Increase in SCP flux from 1960 onward indicates increased atmospheric pollution

49 - Recent decrease in SCP fluxes probably due to air pollution control

50 - Mercury fluxes are relatively high and might reflect local sources of pollution

51

Introduction

Asia has undergone strong economic growth over the last few decades leading to a doubling in regional energy consumption between 1980 and 2003 (Richter et al., 2005; Ohara et al., 2007), with a continuous growth of energy consumption being observed since 2003 (Kurokawa et al., 2013; EANET, 2015). Fossil fuel combustion emits atmospheric pollutants, particularly SO_2, NO_x, CO, non-methane volatile organic compounds, organic carbon, black carbon and trace metals. Although pollutant emissions, particularly from the burning of coal, have been declining in Europe and North America over the last two decades, this has not been the case for much of Asia (Amann et al., 2013; Klimont et al., 2013; Kurokawa et al., 2013). While emissions of SO_2 and particulate matter ($PM_{2.5}$) decreased by 12-15% in East Asia between 2005 and 2010, emissions of NO_x and non-methane volatile organic compounds increased by 15-25% (Wang et al., 2014). Electricity demand in Southeast Asia (SEA), one of the world's fastest developing regions, is projected to be 83% higher in 2035 than in 2011 (International Energy Agency, 2013), with coal providing much of this increased energy demand (Lai et al., 2016).

Increased atmospheric pollution has major implications for society and the environment. An estimated 6.5 million deaths globally each year are attributed to poor air quality (International Energy Agency, 2016; World Health Organization Press, 2016). Koplitz et al. (2017) suggest that the current estimate of around 20,000 ($11.4–28.4 \times 10^3$) excess deaths per year due to emissions from burning coal in SEA will increase to around 70,000 ($40.1–126.7 \times 10^3$) by 2030. Perhaps contrary to common perception (Lai et al., 2016), around 9000 of these excess deaths as a result of increased coal use in SEA are anticipated to occur in China; rising coal emissions in SEA could thus become an increasingly transboundary pollution issue (Koplitz et al., 2017).

Atmospheric greenhouse gas concentrations resulting from fossil fuel combustion are one of the key drivers of anthropogenic climate change (IPCC, 2014), and aerosols (particularly atmospheric black carbon) can significantly influence global radiative forcings (Jacobson, 2001; Streets et al., 2004). Fine aerosol particles can further influence regional climate via surface dimming (Ramanathan et al., 2005; Lau et al., 2006); Fu et al., 2017). Atmospherically deposited pollution places further pressure on anthropogenically impacted wetlands and lowland lakes in SEA, with existing impacts including eutrophication, intensified aquaculture, water abstraction, dam construction, biomass burning, as well as catchment disturbances such as agriculture (e.g. oil palm and other plantations), urbanisation and mining activities (Sharip et al., 2014). Those aquatic ecosystems that have not been severely degraded yield valuable services, such as food and water for local populations and the provision of livelihood opportunities such as eco-tourism (Shuhaimi-Othman et al., 2007; Stockholm International Water Institute, 2009; Sharip and Jusoh, 2010). These services may be difficult to

87 replace. Moreover, human impacted aquatic ecosystems are likely to have significantly reduced

88 biodiversity value (Kopf et al., 2015). Unfortunately, information on the current status of many of

89 these ecosystems, and on the rates and directions of change in environmental conditions over

90 recent decades, is generally lacking. In addition, detailed inventories of anthropogenic energy

91 sources and emissions for Asia only span the last few decades (Kato and Akimoto, 1992; Akimoto

92 2003; Streets et al., 2003; Kurokawa et al., 2013) and their number is comparatively low (Ohara et

93 al., 2007; Rose 2015).

94   Natural archives such as lake sediments have the potential to provide essential information

95 on spatio-temporal variations in fossil fuel consumption in SEA, as spheroidal carbonaceous particles

96 (SCPs), by-products of high-temperature industrial fossil fuel combustion, can be stored in these

97 sediment records following atmospheric deposition, thus tracking changing influx with time (Rose

98 2015). SCPs are fine carbonaceous aerosols, typically 2–50 µm across, formed from the incomplete

99 high-temperature combustion of fossil fuels such as oil and coal (Rose et al., 1994; Rose 2001;

100 Chirinos et al., 2006). SCPs can be transported for thousands of kilometres through the atmosphere

101 under favourable meteorological conditions (Rose et al., 1998; Yang et al., 2001; Inoue et al., 2014),

102 and have been found in remote places such as the Falkland Islands and Antarctica, far removed from

103 the nearest sources (Rose et al., 2012). SCPs are a component of the "black carbon continuum"

104 (Rose, 2008; 2015), but whereas other components of black carbon can be the result of domestic

105 emissions, road transport emissions, or biomass burning (e.g. Kurokawa et al., 2013), SCPs are only

106 formed during high-temperature industrial fossil fuel combustion. As they have no natural sources,

107 SCPs encountered in lake sediment records can be used as indicators of atmospheric deposition

108 from industrial sources (Rose, 2001), especially as they are not susceptible to post-depositional

109 alteration, movement in the sediment column (except by bioturbation), or degradation (Rose et al.,

110 2003). Analysis of SCPs stored in sediments provides a means to reconstruct trends in emissions

111 from the combustion of fossil fuels over time-periods that extend beyond the beginning of

112 documentary and instrumental evidence, which commenced only in the second half of the 20th

113 century and in some regions even more recently (Rose, 2001). Spatial patterns in SCP distribution

114 have been shown to be closely linked to other pollutants, such as sulphur and polycyclic aromatic

115 hydrocarbons (Rose and Juggins 1994; Rose et al., 1998; Barst et al., 2017). A global collation of SCP

116 records includes a disproportionately large number of records from Western Europe and none from

117 SEA (Rose, 2015).

118   Anthropogenic emissions of Hg date back to pre-industrial times, but global Hg emission

119 rates have tripled over the last 150 years, mainly due to increased coal burning (Hylander and Meil,

120 2003; Engstrom et al., 2014; Horowitz et al., 2014; Yang et al., 2016). Aside from industrial sources,

121 there are many additional anthropogenic sources of atmospheric Hg emission, including waste
122 incineration, sulphide ore processing, cement kilns and the production of various metals (Hylander
123 and Meil, 2003). Another important potential source of atmospheric Hg is artisanal and small-scale
124 gold mining (Mason and Pirrone 2009, Cordy et al., 2010). Hg is among the most toxic elements and
125 poses serious threats to both human health and aquatic ecosystems due to its tendency to
126 bioaccumulate and biomagnify through the food chain (Azimi and Moghaddam, 2013; Rice et al.,
127 2014; Okelsrud et al., 2016). Mercury contamination in waterways, sediments and fishes in SEA are
128 already threatening frigate birds as well as other species in the area depending on marine resources,
129 including humans (Mott et al., 2017). With an atmospheric residence time of up to two years
130 (Schroeder and Munthe, 1998), Hg can be released from the atmosphere through both wet and dry
131 deposition. Hg can subsequently be stored in lake and wetland sediments, thereby providing the
132 basis for reconstructions of past variations in pollution loads (e.g. Bindler et al., 2001; Fitzgerald et
133 al., 2005; Yang et al., 2010; Shotyk et al., 2017).

134 Little information on past levels of industry-derived air pollution in SEA is available,
135 especially for the period pre-dating 1980 (US Energy Information; www.eia.gov). This is despite the
136 growing concerns of the effects of local and regional pollution in SEA (Koplitz et al., 2016). This paper
137 addresses this information gap in long-term variations in air pollution deposition in SEA and uses
138 sedimentary evidence as a basis for reconstructing changes in atmospheric pollution in SEA covering
139 the period from the start of industrial fuel consumption to the present, including the time interval
140 before 1980 where data on atmospheric pollution levels are otherwise scarce.

141

142 **Materials and methods**

143 <u>Sites and sampling</u>

144 Using logistical criteria such as site-accessibility and geographical spread, we selected sites from
145 three countries in SEA in order to develop a regional reconstruction of atmospheric deposition
146 pollution history: (1) sediment cores were obtained from three lakes in the Philippines (Yambo,
147 Mohicap, Sampaloc) from the Seven Crater Lakes, a tight cluster of maar crater lakes located near
148 San Pablo City, Laguna Province, on the island of Luzon (Fig. 1). The lakes are presumed to have
149 formed through an explosive phreatic eruption from Mount Banahaw-San Cristobal (Brillo, 2016).
150 The lakes are all moderately deep (>25 m water depth) and have surface areas ranging from 0.23 to
151 1.04 km^2 (Supplementary Table 1) (Aquino, 1983; Laguna Lake Development Authority, 2008). Lakes
152 in the cluster are currently used for aquaculture across a range of intensities; those selected for this
153 study range from relatively pristine (low level of aquaculture; Yambo) to heavily impacted (intensive
154 aquaculture; Sampaloc). (2) Tasik Chini, a flood pulse wetland ecosystem in the state of Pahang,

155 Peninsular Malaysia, consists of 12 shallow, interconnected lake basins (Shuhaimi-Othman et al.,

156 2007). The lake is under strong ecological pressure due to a range of anthropogenic activities in the

157 area, including deforestation for rubber and oil palm plantations, mining, and artificial damming of

158 the lake (Sharip and Jusoh, 2010). (3) There are no natural freshwater ecosystems with long

159 sediment records available for study in Singapore. Instead, we sampled a reservoir (SR)[1], located in

160 the largely forested Central Catchment of Singapore. Construction of SR began in 1970 with

161 damming of the valley upstream of an existing reservoir (Public Utilities Board Website;

162 http://www.pub.gov.sg).

163   Fieldwork was carried out in 2015 (Malaysia) and 2016 (the Philippines, Singapore). For each

164 of our five selected sites we recovered a sediment core from the deepest part of the basin using a

165 UWITEC gravity corer with an inner diameter of 86 mm. As the recovered sediments were highly

166 organic and unconsolidated, core penetration varied between 72-104 cm. All cores preserved the

167 sediment-water interface, and were subsampled in contiguous 1-cm-thick samples in the field.

168

169 <u>Radiometric dating</u>

170 Radiometric dates were obtained for the sediment cores from the Philippines and Malaysia by

171 measuring ^{210}Pb, ^{226}Ra, ^{137}Cs and ^{241}Am using gamma spectrometry; the SR record was not

172 radiometrically dated, although the lowermost part of the sediment core recovered post-dates the

173 onset of reservoir construction (1970). Radiometric dating used freeze-dried sediment samples

174 analysed in ORTEC HPGe GWL series well-type coaxial low background intrinsic germanium detectors

175 at University College London. ^{210}Pb was determined via its gamma emissions at 46.5 keV, and ^{226}Ra

176 by the 295 keV and 352 keV gamma rays emitted by its daughter isotope ^{214}Pb following three weeks

177 of storage in containers (sealed with rubber stops to prevent loss of ^{222}Rn (Pittauerova et al., 2011))

178 to allow radioactive equilibration (Appleby et al., 1986). ^{137}Cs and ^{241}Am were measured by their

179 emissions at 662 and 59.5 keV respectively (Appleby et al., 1986). A constant rate of supply (CRS)

180 model was applied to each sediment core to create an age-depth model (Appleby, 2001). The CRS

181 model assumes a constant rate of unsupported ^{210}Pb supply to the sediment (^{210}Pb derived from

182 atmospheric fallout is unsupported ^{210}Pb), and is one of the most widely used methods for

183 calculating ages based on ^{210}Pb activity (Appleby, 2001).

184

185 <u>SCP analysis</u>

---

[1] The reservoir is anonymized in line with a request from the Public Utilities Board (Singapore) who
kindly granted access to the site

186 The SCP concentration of selected subsamples from all five study sites was determined following the

187 protocol by Rose (1994). Dried sediment subsamples were digested with acids in order to remove

188 organic, siliceous and carbonate sediment fractions. A known volume of processed subsample was

189 then transferred to a coverslip and mounted on a glass microscope slide using Naphrax. SCPs were

190 enumerated using a light microscope and expressed in concentration (number per gram of dry

191 matter (gDM^{-1})). For the sites that were radiometrically dated, SCP concentrations were converted to

192 flux ($n\ cm^{-2}\ yr^{-1}$) to take into account the variability in sediment accumulation rates (Rose et al.,

193 1998). The detection limit for the technique is typically less than 100 gDM^{-1} (Rose, 1994), and

194 concentrations presented here have an accuracy of c. ±30 gDM^{-1} for Tasik Chini and c. ±50-100 gDM^{-1}

195 for the other records. Rose (1994; 2008) provides more details on the SCP preparation protocol and

196 criteria for identification.

197

198 Mercury analysis

199 We measured Hg concentrations in the sediment cores from Sampaloc and Yambo (Philippines)

200 using cold vapour-atomic fluorescence spectrometry (CV-AFS). Samples were digested with 8 mL

201 aqua regia at 100 °C on a hotplate for 2 h in rigorously acid-leached 50 mL polypropylene digestion

202 tubes, along with standard reference materials and sample blanks. The digested solutions (samples,

203 standards and blanks) were subsequently analysed for Hg using CV-AFS following reduction with

204 $SnCl_2$ (Yang et al., 2016). The standard reference material used here (GBW07305; stream sediment)

205 has a certified Hg value of 100 ± 10 $ng\ g^{-1}$; our measured mean value was 103.8 $ng\ g^{-1}$, with a relative

206 standard deviation (RSD) of 3.1 $ng\ g^{-1}$ (n=5).

207

208 Regional climate and atmospheric modelling

209 The monsoonal climate of SEA results in large intra-annual variations in the extent of the air-shed

210 (the area from which a parcel of air, and suspended pollutants, is likely to be sourced) for each of the

211 study sites. This is because seasonal changes in the monsoonal system result in differences in wind

212 direction (Fig. 1) as well as in marked differences in wet and dry periods in most of the region

213 (Supplementary Table 2). Peninsular Malaysia and Singapore are affected by two major monsoon

214 systems, the southwest monsoon (late May-September; Supplementary Table 2) and the northeast

215 monsoon (November-March), which brings high amounts of precipitation. During the transitional

216 months, the equatorial trough lies over Malaysia and winds are generally light and variable. In the

217 Philippines, the summer southwest monsoon brings relatively high amounts of precipitation to most

218 of the archipelago during May-October. The northeast winter monsoon is generally associated with

219 lower quantities of precipitation (Supplementary Table 2). The Philippines are also bisected by a

220　major tropical storm (typhoon) track, generally running east to west, with most major typhoons
221　occurring between June and December (Kubota and Chan, 2009).
222　　　　We analysed potential sources of atmospheric pollution for each of our sites by producing
223　backward trajectories (72 h) of air masses for the Seven Crater Lake region (the Philippines), Tasik
224　Chini (Peninsular Malaysia) and SR (Singapore) following Nagafuchi et al. (2009). The trajectories
225　were plotted using the Hybrid Single-Particle Lagrangian Integrated Trajectory model (HYSPLIT)
226　(Stein et al., 2015; Ready, http://www.ready.noaa.gov) using a weekly sampling resolution for five
227　selected months (May 2016, August 2016, October 2016, November 2016, January 2017) that
228　together represent the different modes of the monsoonal climate in SEA (Supplementary Table 2).
229　The backward trajectory simulations started with air masses at 500 m above the modelled ground
230　levels at starting point; trajectories were calculated based on meteorological data from the Global
231　Data Assimilation System (NOAA, https://www.ready.noaa.gov/gdas1.php).
232
233　**Results**
234　<u>Radiometric dating</u>
235　The unsupported ^{210}Pb profiles show non-monotonic features in the Mohicap, Sampaloc and Tasik
236　Chini records (Supplementary Table 3), confirming the suitability of the CRS model over the
237　alternative, Constant Initial Concentration (CIC) model (Robbins, 1978). Activities of ^{137}Cs and ^{241}Am
238　in these three records are too low to validate ^{210}Pb-based evidence for dating. While the Yambo
239　^{210}Pb profile shows a more regular pattern, small departures from an exponential decline also
240　indicate the use of a CRS dating model for this core. A peak in ^{137}Cs activity at 39.5 cm depth in the
241　Yambo record reflects the 1963 maximum in atmospheric ^{137}Cs fallout resulting from the testing of
242　nuclear weapons. While ^{137}Cs can be mobile in natural environments, it is unlikely that the peak
243　position would have changed. Therefore, the ^{137}Cs peak at 39.5 cm depth is used to correct the CRS
244　^{210}Pb chronology, which initially placed 1963 at 28.5 cm depth. The offset in the ^{210}Pb profile for the
245　Yambo record might be the result of catchment-specific changes in sedimentation processes (such as
246　changes in catchment erosion/inputs or sediment focussing) that might have changed the input of
247　supported ^{210}Pb.
248　　　　The resulting core chronologies (Fig. 2) suggest relatively high sedimentation rates at
249　Mohicap, with an increase in rate of sedimentation between 1940 and 1970, followed by a uniform
250　rate of 0.21 g cm^{-2} yr^{-1}. The Sampaloc record shows an increase in sedimentation rate around 1995,
251　whereas the Yambo record shows relatively stable rates throughout. Rates of sedimentation are
252　most variable in the Tasik Chini record, where step-wise increases can be seen around 1945 and
253　2000, with considerable variations during the last decade.

254

SCP records

256 Concentrations of SCPs in the three records from the Philippines and the record from Malaysia show
257 similar trends, with first occurrences being observed in samples taken from the lower part of each
258 core, followed by increasing concentrations in samples from higher in the sequence (Fig. 3). All
259 records show decreasing concentrations in the uppermost part of the core. The concentrations differ
260 from core to core, with maximum values reaching c. 40,000 SCPs gDM^{-1} at Sampaloc, but only c. 300
261 SCPs gDM^{-1} at Tasik Chini. The SR record shows continuous presence of SCPs from the onset of the
262 core, with initial concentrations of SCPs of c. 800 SCPs gDM^{-1} around 70 cm core depth, subsequently
263 increasing to maximum concentrations of c. 6000 SCPs gDM^{-1} at 45 cm core depth and with
264 concentrations fluctuating between 2000-6000 SCPs gDM^{-1} in the upper part of the record.

265 First occurrences of SCPs often reflect early developments in the industrial combustion of
266 coal and oil, and following two earlier samples with single occurrences of SCPs (Fig. 3) the Tasik Chini
267 SCP flux record dates the onset of continuous presence of SCPs in sediment samples to c. 1950 (Fig.
268 4). The age-depth models of the cores from the Philippines do not reach back far enough to date first
269 occurrences, and hence the SCP flux profiles are truncated. The Sampaloc record indicates that SCPs
270 are encountered earlier than at Tasik Chini, with SCPs in the oldest sediment sample dated to c.
271 1925. The four radiometrically dated records all show increased SCP fluxes around 1960, although
272 fluxes at Tasik Chini are much lower (10 cm^{-2} yr^{-1}) than the values observed at the Philippine sites
273 (1000 cm^{-2} yr^{-1}). Three of the four records show a second step-change increase in SCP flux around
274 1990, with all records showing maximum flux at around 2000. All four records subsequently show
275 decreasing flux to the present.

276

Mercury

278 Hg concentrations range between 30 and 150 ng g^{-1} in the Sampaloc and Yambo records (Fig. 5). In
279 the core from Sampaloc, maximum concentrations of 90-150 ng g^{-1} are reached between 30 and 55
280 cm depth. Hg concentrations were initially low in Yambo (30-40 ng g^{-1} below 70 cm depth in the
281 core), followed by relatively stable concentrations of 50-90 ng g^{-1} for the upper part of the record.
282 When converted to flux, Hg in Sampaloc is around 40 µg m^{-2} yr^{-1} for most of the sequence, with an
283 increase to values over 80 µg m^{-2} yr^{-1} between 1990 and 2005. The Yambo record initially shows a Hg
284 flux of 60-90 µg m^{-2} yr^{-1} prior to 1965, after which it shows a relatively stable flux of c. 110 µg m^{-2} yr^{-1}.

285

Atmospheric modelling

287   Atmospheric modelling (Fig. 1) indicates seasonal differences in the air masses reaching our study

288   sites throughout the year. The winter monsoon (November-April; Supplementary Table 2) delivers

289   air masses from mainly the east-northeast. While this means that air masses affecting the study sites

290   in the Philippines mainly pass over the Philippine Sea, some of the backward trajectories suggest

291   that southern Japan could also be a source of atmospheric pollution (e.g. Fig. 1c). As November-April

292   is a period with relatively low precipitation in the Philippines, the chances for rain-out of

293   atmospheric particles are lower, and airborne particles can potentially be transported further. In

294   contrast, during June-September air masses over the Philippines arrive from the west, bringing

295   relatively high amounts of precipitation. The modelling results suggest that there is only limited

296   scope for airborne particle sources from outside of the Philippines to arrive at the study sites on the

297   island of Luzon. Seasonal variability is slightly higher for the sites in Peninsular Malaysia and

298   Singapore. Winds from the northeast dominate from October-January, southwestern winds from

299   January-April, and southeasterly winds from May-September (Supplementary Table 2). Highest

300   amounts of precipitation are commonly observed during the northeast monsoon (November-March)

301   for eastern Peninsular Malaysia, suggesting that although the three-day trajectories cover large

302   distances for these months, reaching as far as the South China Sea and the Indian Ocean (Fig 1c),

303   airborne particles have a higher chance of raining out during this part of the year. The different

304   directions of the air mass trajectories, in addition to the length of the three-day pathways, suggest

305   that the sediment records of our sites represent a regionally integrated signal of air pollution, and

306   that SCPs transported to our site could be partly derived from long-range transport (with travel

307   distances potentially exceeding 10^3 km). However, the modelling results also suggest that for large

308   parts of the year air masses mainly pass over open water, and combined with information on

309   seasonality of precipitation, indicate that most of the airborne particles are probably derived from

310   local sources.

311

312   **Discussion**

313   <u>Spatio-temporal trends of SCP fluxes</u>

314   Burning of fossil fuels in SEA started toward the end of the 19th century albeit on a small scale. The

315   first coal-fired power plant in the Philippines was built in Manila, also on the island of Luzon, in 1892

316   (Ongsotto and Ongsotto, 2002), and this and other power plants constructed in the vicinity of Manila

317   could account for the early detection of SCPs in the record from Sampaloc (Fig. 4), located around

318   100 km to the south. Extensive and region-wide fossil fuel consumption did not begin until c. 1950-

319   1960, when all four ^{210}Pb-dated records show an increase in SCP flux. The use of fossil fuels was

320   locally stimulated by legislation such as the Oil Exploration and Development Act (1972) of the

321 Philippines, which offered tax exemptions for oil exploration and exploitation. The increase in coal

322 and oil consumption after 1980 in SEA (Fig. 4b) is mirrored in the increase in SCP flux in the records

323 of Yambo, Sampaloc and Tasik Chini, which all show a phase of SCP flux during the 1980s. A further

324 increase in coal and oil consumption after 2000 (IEA, 2013; Kurokawa et al., 2013) is not reflected in

325 the SCP records, which all show decreasing flux from that time. This divergence in trends might be

326 the result of the implementation of air pollution control measures (Wang et al., 2014; Mohktar et al.,

327 2014). For instance, an expansion of air pollution control measures in the Philippines followed

328 implementation of the Philippines Clean Air Act of 1999 (Republic Act No. 8749), which set pollution

329 emission limitations for the fossil fuel industry (as well as for motor vehicles). Implementation of air

330 pollution control policies commenced in China from 1980 onward, but only became effective from c.

331 2005 onward (Yin et al., 2016). In Malaysia, the Malaysia Environmental Quality (Clean Air) of 1978

332 provided the first regulations relating to atmospheric pollution control, only recently being replaced

333 by the New Environmental Quality (Clean Air) Regulation 2014. Despite these intra- and inter-

334 regional differences in the timing of the introduction of air pollution control measures in Southeast

335 and East Asia, their implementation was more strenuously enforced only from c. 2000 onward, and

336 this is in line with our observed decrease in SCP fluxes in SEA.

337   Historical records of monthly precipitation amounts show a slight increase in rainfall in

338 Malaysia from the 1990s onward (Climate Change Knowledge Portal,

339 http://sdwebx.worldbank.org/climateportal), with the strongest increases in rainfall amounts seen

340 during the northeast monsoon season (November-March). This increase in precipitation amounts

341 could have resulted in more effective rain-out of particulates, and shortened transport distances for

342 airborne particulates such as SCPs (e.g. Ruppel et al., 2013; Supplementary Figure 1). This would

343 have decreased the amount of regionally-derived SCPs for some of our sites from c. 1990. It is

344 however difficult to disentangle the potential effects of an increase in precipitation amounts from

345 the effects of increasingly more effective air pollution control measures, as both would result in

346 decreased SCP fluxes to our sites. More research is needed to differentiate between the effects of

347 these two drivers of changes in SCP deposition at our sites.

348   Individual SCP flux records were standardised and combined in a regional summary record

349 for SEA (Fig. 4c). The curve that is shown in Fig. 4c is dominated by the results from the Philippines,

350 and is currently based on a relatively low number of records that are available for comparison.

351 Future results from SEA might alter the general trend of the record shown in Fig. 4c. However, the

352 current summary diagram resembles trends observed in extra-tropical parts of Asia, such as China

353 and Japan. For instance, the record for Akani-konuma, a remote high-altitude lake in Japan, shows

354 first occurrences of SCPs around the early 1950s, before reaching peak flux around the late-1980s

355 (Nagafuchi et al., 2009). SCP concentration data from the middle Yangtze in China show an abrupt

356 increase in the early 1950s, before declining from around 2000, while similar data from Beijing show

357 a much more recent (late 1980s) increase, with the predominant morphology of SCPs indicating the

358 combustion of coal as the main source (Wu et al., 2005; Hirakawa et al., 2011). By comparison,

359 sediment cores from lakes Taihu and Donghu in eastern China both exhibit first occurrences of SCPs

360 in the 1930s before showing rapid increases in SCP deposition around 1950 and peak flux at around

361 1990 (Rose, 2015). A similar pattern of accumulation is also shown in coastal sediments from Japan

362 (Murakami-Kitase et al., 2010; Hirakawa et al., 2011). Sediment samples from the sub-aqueous part

363 of the Yangtze Delta and dating to before the 1930s contain SCPs, with concentrations rising steeply

364 in the early 1950s (Wang et al., 2014). The similar trends observed in our records and in the

365 published records from Japan and China reflect the simultaneous expansion of fossil fuel combustion

366 around this time. Rose (2015) provides a global synthesis of SCP records, illustrating that while

367 certain parts of the world are well-studied (e.g. Europe), tropical regions are not, hampering our

368 understanding of past atmospheric pollution patterns. Rose (2015) shows a normalised summary

369 curve for Asia that includes 10 sites, but these sites cover a geographical range spanning from the

370 northern Urals in Arctic Russia in the northwest (Solovieva et al., 2005) to Japan in the southeast

371 (Yoshikawa et al., 2000; Nagafuchi et al., 2009), and all are located outside of tropical Asia. The

372 summary curve for Asia (Rose, 2015) shows relatively low abundances or absence of SCPs pre-1950,

373 followed by a trend of increasing flux from the mid-1950s to a peak around 1990. Inferred variations

374 in atmospheric pollution levels for SEA are thus generally in line with information on fossil fuel usage

375 in East and Southeast Asia (Ohara et al., 2007; Wang et al., 2014). While not outside of the range of

376 dating uncertainties there are, however, slight differences in the SCP flux records from the two

377 regions, with peak values being reached in East Asia at c. 1990 (Rose, 2015) but around 2000 in SEA

378 (this study). In addition, the individual records from East Asia show decadal-scale differences when

379 compared with each other as well. On a global scale, most SCP records show a more abrupt increase

380 immediately after c. 1950, reaching peak flux values one or two decades earlier than the peak values

381 as seen in our records. This likely reflects regional differences in development and pollution

382 mitigation.

383 While future projections of black carbon emissions suggest globally decreasing

384 concentrations, regional estimates differ between a slight increase (Streets et al., 2004) and a

385 decrease (Wang et al., 2014) for SEA. The more recent estimates of a decrease in future emissions

386 take into account substantial measures taken by local governments to reduce air pollution with the

387 objectives of climate change mitigation as well as air quality improvement, such as the

388 Environmental Quality (Clean Air) Regulation of 2014 in Malaysia (Mohktar et al., 2014; Wang et al.,

389   2014). Our results suggest that strict implementation of these regulations would lead to continued

390   declines in SCP deposition. In contrast, the Philippine Energy Plan (PEP) 2012-2030 seeks to achieve

391   energy independence through the use of indigenous fuel resources, including but not limited to

392   indigenous coal and oil fields. This suggests that the Philippines will remain dependent on

393   conventional fuels for the foreseeable future, thus affecting future SCP emissions in the region.

394

395   Potential sources of SCPs

396   While the patterns of variations in SCP loads are similar between the study sites, the absolute fluxes

397   vary substantially. For instance, our records show that maximum flux at Tasik Chini only reaches 40

398   cm^{-2} yr^{-1}, whereas maximum flux in the Philippines reaches c. 2000 cm^{-2} yr^{-1}. SCP fluxes can vary over

399   short distances (Rose and Appleby, 2005; Rose, 2015) and catchment- and site-specific processes like

400   wind fetch, exposure, catchment slope, vegetation coverage and sediment transport all influence

401   the extent to which SCPs accumulate in lake sediments, explaining some of the high spatial

402   variability noted in other studies. However, proximity to pollution sources is the most likely

403   explanation for the 2-order magnitude difference observed between our sites. Metropolitan Manila,

404   the capital and by far the largest urban conurbation in the Philippines with an estimated population

405   of 13 million, is located about 100 km to the north of the Seven Crater Lakes. San Pablo (population

406   266,000), which extends to the shoreline of Sampaloc, is also a relatively large, densely populated

407   urban area. There are several power plants in the air-shed for the cluster of lakes forming the Seven

408   Crater Lakes (Fig. 1b). While smaller-sized power generation facilities have been in operation from

409   1963 onward, large coal and oil plants came into operation in the 1980s and 1990s. These power

410   plants can serve as local sources of SCPs accumulating in sediments at Mohicap, Sampaloc and

411   Yambo. In contrast, all power plants on Peninsular Malaysia (Fig. 1a) are located on the western side

412   of the peninsula. Tasik Chini therefore receives relatively more long-range emissions than the

413   Philippine sites which receive more short-range transported SCPs.

414

415   Mercury fluxes

416   Global Hg emission rates have tripled since c. 1850, mainly due to increased coal burning (Engstrom

417   et al., 2014; Horowitz et al., 2014). There are however many additional sources of anthropogenic Hg

418   emission, including waste incineration and sulphide ore processing (Hylander and Meil, 2003). An

419   important potential source of atmospheric Hg is artisanal and small-scale gold mining (Mason and

420   Pirrone 2009, Cordy et al., 2010) and an estimated 300,000 people are employed in the small-scale

421   mining sector of the Philippines (Lu, 2012). Artisanal mines have spread throughout the country

422   since the mid-1980s gold-rush, with high numbers on the island of Mindanao to the south of Luzon

423 (Appleton et al., 1999).The expanding practice of artisanal gold mining in SEA is responsible for much

424 of the region's environmental mercury emissions (Pacyna et al., 2010).

425   The first significant increases in Hg in lake sediment cores are typically observed from the

426 mid-19th century, even in remote areas (Muir et al., 2009). While our records do not have age-depth

427 models that reach back to the 19th century, our record from Sampaloc shows an increase in Hg

428 concentrations at c. 65 cm depth. We interpret this increase in concentration as a clear pollution

429 signal, which occurred prior to c. 1925 (37 cm depth), the start of our chronology. The declining

430 trend in Hg concentrations at Sampaloc is related to dilution as a result of increased sedimentation

431 rates, as Hg flux increases from c. 1925 (Fig. 5). Similarly, Hg concentrations at Yambo increase from

432 85 cm onward, which is sometime before the c. 1950 (47 cm depth) onset of the sediment

433 chronology for this site. The observed values of c. 40-110 $\mu g\ m^{-2}\ yr^{-1}$ compare well to modern

434 observations of wet deposition fluxes of total Hg in China, which ranges between 24.9 and 39.6 μg

435 $m^{-2}\ yr^{-1}$ for five study sites in the Wujiang River basin, but are much higher than observations of wet

436 deposition fluxes for Europe and North America (Guo et al., 2008; Yang et al., 2009). However,

437 comparison of fluxes derived from different types of observations as well as from different areas will

438 be hampered by the difference in sources of input, as well as differences in the human impact on the

439 landscape (e.g. deforestation). While the SCPs encountered in our records might reflect a local or

440 regional source of pollution, the early increases in Hg concentrations most likely indicate a larger

441 regional or even global impact, in line with observations elsewhere (Fitzgerald et al., 2005; Muir et

442 al., 2009; Yang et al., 2010). The presence of artisanal gold mining as well as other small-scale mining

443 activities will likely have provided additional local inputs of Hg.

444

445 <u>Impact of atmospheric pollution on Southeast Asian wetlands</u>

446 Lakes and wetland ecosystems are not equally vulnerable to pollution because of their differing

447 ability to buffer the effects of pollutants, but little is known of the buffering capacity of aquatic

448 ecosystems in SEA. Alkalinity of waters from Tasik Chini is rather low (0.05-0.20 meq L^{-1}; unpubl.

449 data), and thus poorly buffered and susceptible to acidification. The results of a region-wide

450 precipitation monitoring project show that precipitation has an annual average pH of <5.0 for large

451 parts of SEA, with sulphuric acid the main cause of acidification (EANET, 2011). Lake monitoring data

452 for sites in Malaysia and Indonesia provide evidence for declining lake-water pH and increasing

453 sulphate (SO_4^{2-}) concentration, although the cause of apparent acidification remains unknown

454 (EANET, 2011; Sase et al., 2017). Combined with other pressures on water quality (e.g. sewerage

455 inputs from urban areas, fish farming, catchment disturbance, climate change), acidification poses a

456 severe risk to aquatic ecosystem functioning and service provision in SEA, and indeed tropical Asia

457 more widely.

458   SCP fluxes in SEA have declined over the last two decades (Fig. 4), likely as a result of the

459 introduction of particle-arrestor technologies and improved pollution mitigation policies for

460 industrial fuel combustion. In contrast, Hg fluxes at these lakes (Fig. 5) have remained relatively

461 constant across the second half of the 20th century to the present. Hg concentrations show a

462 decreasing trend in Sampaloc, potentially related to dilution through increased sedimentation rates,

463 and have remained stable at Yambo, despite the observed increase in sedimentation rates. While

464 several pollution controls have constrained emissions of atmospheric Hg from e.g. power generation

465 and cement production (Zhao et al., 2015), the more diverse sources of Hg, including artisanal

466 mining, might explain the absence of a decrease in sedimentary Hg concentrations in the Yambo

467 record.

468   The increased sedimentation rates at Sampaloc and Yambo could partially reflect elevated

469 levels of catchment soil erosion. This soil material includes Hg from atmospheric deposition over

470 time, and is thus a source of delayed input of Hg (Yang et al., 2016). Hg flux to these lakes can

471 therefore be expected to remain high for decades to come, even following the implementation of

472 mitigation measures such as those associated with the Minamata Convention (Ha et al., 2017).

473 Transfer of Hg may therefore have potentially long-lasting impacts on aquatic and human health.

474

475 **Conclusions**

476 We used lake sediment archives to reconstruct trends in atmospheric pollution levels across SEA,

477 covering the period from the start of industrial fuel consumption to the present. First occurrences of

478 SCPs, reflecting early developments in the industrial combustion of coal and oil, are dated to c. 1950

479 at Tasik Chini (Malaysia) and are shown to predate c. 1925 at Sampaloc (Philippines). All SCP records

480 show increasing fluxes from 1960 onward, indicating the onset of extensive and region-wide fossil

481 fuel consumption. Increases in SCP fluxes between 1960 and 2000 reflect the increases in fossil fuel

482 consumption in SEA, whereas the decreasing SCPs fluxes between 2000 and the present might be

483 the result of the implementation of air pollution control measures. Atmospheric modelling suggests

484 that most of the airborne particles are derived from local or regional sources. The trends observed in

485 our SCP flux data compare well to independent records from extra-tropical parts of Asia, although

486 peak flux is reached slightly later in SEA (around 2000) when compared to records from China and

487 Japan (c. 1990).

488   The Sampaloc record shows an increase in Hg concentrations prior to c. 1925, the start of

489 our chronology, which is interpreted as a clear pollution signal. Both the Sampaloc and the Yambo

490   record show relatively high Hg fluxes with maximum fluxes reaching 90-110 µg m^{-2} yr^{-1}. The

491   reconstructed fluxes compare well to observations from China, but are higher than recent Hg

492   deposition rates observed in Europe and North America. Whereas the SCPs encountered in our

493   records might reflect a regional source of pollution, the early increases in Hg concentrations most

494   likely indicate a larger regional or even global impact. The extensive presence of artisanal mining

495   activities in the Philippines will likely have provided additional local inputs of Hg.

496

506

507   **Supporting Information**. Table S1 presents site information for the five study sites presented in this

508   manuscript. Table S2 provides information on monthly wind (Table S2a) and precipitation (Table

509   S2b) amounts for Singapore, Malaysia and the Philippines. Table S3 provides the ^{210}Pb measurement

510   data for the four radiometrically dated profiles. Figure S1 shows altitudes of air masses during the 72

511   hours prior to arriving at our sites for five selected dates (cf the data shown in Fig. 1c-11g)

512

513   **References**

514   Akimoto H (2003) Global air quality and pollution. Science 302, 1716-1719.

515   Amann M, Klimont Z, Wagner F (2013) Regional and Global Emissions of Air Pollutants: Recent

516   Trends and Future Scenarios. Annu. Rev. Environ. Resour. 38, 31–55.

517   Appleby PG, Nolan PJ, Gifford DW, Godfrey MJ, Oldfield F, Anderson NJ, Battarbee RW (1986) ^{210}Pb

518   dating by low background gamma counting. Hydrobiologia 141, 21-27.

519   Appleby PG (2001) Chronostratigraphic techniques in recent sediments. In Tracking Environmental

520   Change Using Lake Sediments. Vol. 1: Basin Analysis, Coring and Chronological Techniques;

521   Last, W. M., Smol, J. P., Eds.; Kluwer: Dordrecht; pp 171–203.

522   Appleton JD, Williams TM, Breward N, Apostol A, Miguel J, Miranda C (1999) Mercury contamination
523   associated with artisanal gold mining on the island of Mindanao, the Philippines. Sci. Total
524   Environ. 228, 95-105.

525   Aquino LV (1983) Using Spheroidal Carbonaceous Particles in lake sediments as a stratigraphic
526   marker for the Anthropocene, Philippines. M.Sc. Dissertation, University of the Philippines,
527   Iloilo City, Philippines.

528   Azimi S, Moghaddam MS (2013) Effect of mercury pollution on the urban environment and human
529   health. Environ. Ecol. Res. 1, 12-20.

530   Barst BD, Ahad JME, Rose NL, Jautzy JJ, Drevnick PE, Gammon PR, Sanei H, Savard MM (2017) Lake-
531   sediment record of PAH, mercury, and fly-ash particle deposition near coal-fired power
532   plants in Central Alberta. Environ. Pollut. 231, 644-653.

533   Bindler R, Renberg I, Appleby PG, Anderson NJ, Rose NL (2001) Mercury accumulation rates and
534   spatial patterns in lake sediments from west Greenland: a coast to ice margin transect.
535   Environ. Sci. Technol. 35, 1736-1741.

536   Brillo BBC (2016) Developing Mohicap Lake, San Pablo City, Philippines. Soc. Sci. 11, 283-290.

537   Chirinos L, Rose NL, Urrutia R, Muñoz P, Torrejón PF, Torres L, Cruces F, Araneda A, Zaror C (2006)
538   Environmental evidence of fossil fuel pollution in Laguna Chica de San Pedro lake sediments
539   (Central Chile). Environ. Pollut. 141, 247-256.

540   Cordy P, Veiga MM, Salih I, Al-Saadi S, Console S, Garcia O, Mesa LA, Velásquez-López PC, Roeser M
541   (2011) Mercury contamination from artisanal gold mining in Antioquia, Colombia: The
542   world's highest per capita mercury pollution. Sci. Total Environ. 410-411, 154-160.

543   EANET (2011) *The second periodic report on the state of acid deposition in East Asia*; Acid Deposition
544   Monitoring Network in East Asia. Acid Deposition Monitoring Network in East Asia (EANET)

545   EANET (2015) *Review on the State of Air Pollution in East Asia*. Acid Deposition Monitoring Network
546   in East Asia (EANET)

547   Engstrom DR, Fitzgerald WF, Cooke CA, Lamborg CH, Drevnick PE, Swain EB, Balogh SJ, Balcom PH
548   (2014) Atmospheric Hg emissions from preindustrial gold and silver extraction in the
549   Americas: A reevaluation from lake-sediment archives. Environ. Sci. Technol. 48, 6533-6543.

550   Fitzgerald WF, Engstrom DR, Lamborg CH, Tseng CM, Balcom PH, Hammerschmidt CR (2005) Modern
551   and historic atmospheric mercury fluxes in northern Alaska: global sources and Arctic
552   depletion. Environ. Sci. Technol. 39, 557-568.

553   Fu C, Ding A, Wu J (2017) Review on Studies of Air Pollution and Climate Change Interactions in
554   Monsoon Asia. In: Chang C-P, Kuo H-C, Lau N-C, Johnson RH, Wheeler MC (Eds) *The Global
555   Monsoon System: Research and Forecast 9*. pp 315-327.

556   Guo Y, Feng X, Li Z, He T, Yan H, Meng B, Zhang J, Qiu G (2008) Distribution and wet deposition fluxes
557   of total and methyl mercury in Wujiang River Basin, Guizhou, China. Atmosph. Environ. 42,
558   7096-7103.

559   Ha E, Basu N, Bose-O'Reilly S, Dorea JG, McSorley E, Sakamoto M, Chan HM (2017) Current progress
560   on understanding the impact of mercury on human health. Environ. Res. 152, 419-433.

561   Hirakawa H, Muralami-Kitase A, Okudaira T, Inoue J, Yamazak H, Yoshikawa S (2011) The spatial and
562   temporal distributions of spheroidal carbonaceous particles from sediment core samples
563   from industrial cities in Japan and China. Environ. Earth Sci. 64, 833-840

564   Horowitz HM, Jacob DJ, Amos HM, Streets DG, Sunderland EM (2014) Historical Mercury Releases
565   from Commercial Products: Global Environmental Implications. Environ. Sci. Technol. 48,
566   10242-10250.

567   Hylander LD, Meil IM (2003) 500 years of mercury production: global annual inventory by region
568   until 2000 and associated emissions. Sci. Total Environ. 304, 13-27.

569   Inoue J, Momose A, Okudaira T, Murakami-Kitase A, Yamazaki H, Yoshikawa S (2014) Chemical
570   compositions of Northeast Asian fly ash particles: Implications for their long-range
571   transportation. Atmos. Environ. 95, 375-382.

572   Intergovernmental Panel on Climate Change (2014) *Climate Change 2014: Synthesis Report.*
573   Contribution of Working Groups I, II and III to the Fifth Assessment Report of the
574   Intergovernmental Panel on Climate. Geneva, Switzerland.

575   International Energy Agency (2013) *Southeast Asia Energy Outlook. World Energy Outlook Special*
576   *Report.* Paris, France.

577   International Energy Agency (2016) *Energy and air pollution. World Energy Outlook – Special report.*
578   Paris, France.

579   Jacobson MZ (2001) Strong radiative heating due to the mixing state of black carbon in atmospheric
580   aerosols. Nature 409, 695– 697.

581   Kato N, Akimoto H (1992) Anthropogenic emissions of SO_2 and NO_x in Asia: emissions inventories,
582   Atmos. Environ. 26, 2997–3017.

583   Klimont Z, Smith SJ, Cofala J (2013) The last decade of global anthropogenic sulfur dioxide:
584   2000−2011 emissions. Environ. Res. Lett. 8, 014003.

585   Kopf RK, Finlayson CM, Humphries P, Sims NC, Hladyz S (2015) Anthropocene baselines: assessing
586   change and managing biodiversity in human-dominated aquatic ecosystem. Biosci 65, 798-
587   811.

588   Koplitz SN, Mickley LJ, Marlier ME, Buonocore JJ, Kim PS, Liu T, Sulprizio MP, DeFries R, Jacob DJ,
589   Schwartz J, Pongsiri M, Myers S (2016) Public health impacts of the severe haze in Equatorial

590   Asia in September–October 2015: demonstration of a new framework for informing fire
591   management strategies to reduce downwind smoke exposure. Environ. Res. Lett. 11,
592   094023.

593 Koplitz SN, Jacobs DJ, Sulprizio MP, Myllyvirta L, Reid C (2017) Burden of Disease from Rising Coal-
594   Fired Power Plant Emissions in Southeast Asia. Environ. Sci. Technol. 51, 1467-1476.

595 Kubota H, Chan JCL (2009) Interdecadal variability of tropical cyclone landfall in the Philippines from
596   1902 to 2005. Geophys. Res Lett. 36, L12802.

597 Kurokawa J, Ohara T, Morikawa T, Hanayama S, Janssens-Maenhout G, Fukui T, Kawashima K,
598   Akimoto H (2013) Emissions of air pollutants and greenhouse gases over Asian regions
599   during 2000-2008: Regional Emission inventory in Asia (REAS) version 2. Atmos. Chem. Phys.
600   13, 11019-11058.

601 Laguna Lake Development Authority-Environmental Quality Management Division (2008) *Water
602   Quality Report of the Seven Crater Lakes 2006-2008.* Rizal, Philippines.

603 Lai I-C, Lee C-L, Huang H-C (2016) A new conceptual model for quantifying transboundary
604   contribution of atmospheric pollutants in the East Asia Pacific rim region. Environ. Internat.
605   88, 160-168.

606 Lau KM, Kim MK, Kim KM (2006) Asian summer monsoon anomalies induced by aerosol direct
607   forcing: The role of the Tibetan Plateau. Clim. Dynam. 26, 855–864.

608 Lu JL (2012) Occupational health and safety in small scale mining: focus on women workers in the
609   Philippines. J Internat. Women's Studies 13, 103-113.

610 Mason R, Pironne N (2009) *Mercury Fate and Transport in the Global Atmosphere Emissions,
611   Measurements and Models.* Springer US, New York

612 Mohktar MM, Taib RM, Hassim MH (2014) Understanding selected trace elements behavior in a
613   coal-fired power plant in Malaysia for assessment of abatement technologies. J Air & Waste
614   Manag. Assoc. 64, 867–878.

615 Mott R, Herrod A, Clarke RH (2017) Post-breeding dispersal of frigatebirds increases their exposure
616   to mercury. Mar. Pollut. Bull. 119, 204-210.

617 Muir DCG, Wang X, Yang F, Nguyen N, Jackson TA, Evans MS, Douglas M, Kock G, Lamoureux S,
618   Pienitz R, Smol JP, Vincent WF, Dastoor A (2009) Spatial trends and historical deposition of
619   mercury in eastern and northern Canada inferred from lake sediment cores. Environ. Sci.
620   Technol. 43, 4802-4809.

621 Murakami-Kitase A, Okudaira T, Inoue J, (2010) Relationship between surface morphology and
622   chemical composition of spheroidal carbonaceous particles within sediment core samples
623   recovered from Osaka Bay Japan. Environ. Earth Sci. 59, 1723–1729

624 Nagafuchi O, Rose NL, Hoshika A, Satake K (2009) The temporal record and sources of
625   atmospherically deposited fly-ash particles in Lake Akagi-konuma, a Japanese mountain lake.
626   J. Paleolimnol. 42, 359-371.

627 Ohara T, Akimoto H, Kurokawa J, Horii N, Yamaji K, Yan X, Hayasaka T (2007) An Asian emission
628   inventory of anthropogenic emission sources for the period 1980-2020. Atmosph. Chem.
629   Phys. 7, 4419-4444.

630 Okelsrud A, Lydersen E, Fjeld E (2016) Biomagnification of mercury and selenium in two lakes in
631   southern Norway. Sci. Total Environ. 566, 596-607.

632 Ongsotto RR, Ongsotto RR (2002) Philippine history module-based learning, 1st ed; Rex Book Store:
633   Manilla.

634 Pacyna EG, Pacyna JM, Sundseth K, Munthe J, Kindbom K, Wilson S, Steenhuisen F, Maxson P (2010)
635   Global emission of mercury to the atmosphere from anthropogenic sources in 2005 and
636   projections to 2020. Atmosph. Environ. 44, 2487-2499.

637 Pittauerová D, Hettwig B, Fischer HW (2011) Pb-210 sediment chronology: Focused on supported
638   lead. Radioprotection 46, S277-S282.

639 Ramanathan V, Chung C, Kim D, Bettge T, Buja L, Kiehl JT, Washington WM, Fu Q, Sikka DR, Wild M
640   (2005) Atmospheric brown clouds: impact on South Asian climate and hydrologic cycle. P.
641   Natl. Acad. Sci. 102, 5326–5333.

642 Rice KM, Walker EM Jr, Wu M, Gillette C, Blough ER (2014) Environmental mercury and its toxic
643   effects. J. Prev. Med. Public Health 47, 74-83.

644 Richter A, Burrows P, Nues H, Granier C, Niemeijer U (2005) Increase in tropospheric nitrogen
645   dioxide over China observed from space. Nature 437, 129–130.

646 Robbins JA (1978) Geochemical and geophysical applications of radioactive lead. Biogeochem. Lead
647   Environ. 1, 285-337.

648 Rose NL (1994) A note on further refinements to a procedure for the extraction of carbonaceous fly
649   ash particles from sediments. J. Paleolimnol. 11, 201–204.

650 Rose NL (2001) Fly ash particles. In: Tracking Environmental Change Using Lake Sediments, Vol. 2.
651   Physical and Chemical Techniques; Last, W. M., Smol, J. P., Eds.; Kluwer Academic Publishers:
652   Dordrecht, pp. 319–349.

653 Rose NL (2008) Quality control in the analysis of lake sediments for spheroidal carbonaceous
654   particles. Limnol. Oceanogr. Methods 6, 172-179.

655 Rose NL (2015) Spheroidal Carbonaceous Fly Ash Particles Provide a Globally Synchronous
656   Stratigraphic Marker for the Anthropocene. Environ. Sci. Technol. 49, 4155-4162.

657   Rose NL, Appleby PG (2005) Regional applications of lake sediment dating by spheroidal
658   carbonaceous particle analysis I. United Kingdom. J. Paleolimnol. 34, 349-361.

659   Rose NL, Juggins S (1994) A spatial relationship between carbonaceous particles in lake sediments
660   and sulphur deposition. Atmosph. Environ. 28, 177-183.

661   Rose NL, Juggins S, Watt J, Battarbee R (1994) Fuel-type characterisation of spheroidal carbonaceous
662   particles using surface chemistry. Ambio. 23, 296-299.

663   Rose NL, Appleby PG, Boyle JF, Mackay AW, Flower RJ (1998) The spatial and temporal distribution
664   of fossil-fuel derived pollutants in the sediment record of Lake Baikal, eastern Siberia. J.
665   Paleolimnol. 20, 151-162.

666   Rose NL, Flower RJ, Appleby PG (2003) Spheroidal carbonaceous particles (SCPs) as indicators of
667   atmospherically deposited pollutants in North African wetlands of conservation importance.
668   Atmosph. Environ. 37, 1655–1663.

669   Rose NL, Jones VJ, Noon PE, Hodgson DA, Flower RJ, Appleby PG (2012) Long-range transport of
670   pollutants to the Falkland Islands and Antarctica: Evidence from lake sediment fly-ash
671   particle records. Environ. Sci. Technol. 46, 9881-9889.

672   Ruppel M, Lund MT, Grythe H, Rose NL, Weckström J, Korhola A (2013) Comparison of Spheroidal
673   Carbonaceous Particle Data with Modelled Atmospheric Black Carbon Concentration and
674   Deposition and Air Mass Sources in Northern Europe, 1850–2010. Adv. Meteorol. 2013,
675   Article ID 393926, http://dx.doi.org/10.1155/2013/393926.

676   Sase H, Yamashita N, Luangjame J, Garivait H, Kietvuttinon B, Visaratana T, Kamisako M, Kobayashi
677   R, Ohta S, Shindo J, Hayashi K, Toda H, Matsuda K (2017) Alkalinization and acidification of
678   stream water with changes in atmospheric deposition in a tropical dry evergreen forest of
679   northeastern Thailand. Hydrol. Proc. 31, 836–846.

680   Schroeder WH, Munthe J (1998) Atmospheric mercury – an overview. Atmosph. Environ. 32, 809-
681   822.

682   Sharip Z, Jusoh J (2010) Integrated lake basin management and its importance for Lake Chini and
683   other lakes in Malaysia. Lakes Reservoirs: Res. Manag. 15, 41–51.

684   Sharip Z, Zaki ATA, Shapai MAHM, Suratman S, Shaaban AJ (2014) Lakes of Malaysia: Water quality,
685   eutrophication and management. Lakes Reservoirs: Res. Manag. 19, 130–141.

686   Shotyk W, Appleby PG, Bicalho B, Davies LJ, Froese D, Grant-Weaver I, Magnan G, Mullan-Boudreau
687   G, Noemberg T, Pelletier R, Shannon B, van Bellen S, Zaccone C (2017) Peat bogs document
688   decades of declining atmospheric contamination by trace metals in the Athabasca
689   Bituminous Sands Region. Environ. Sci. Technol. 51, 6237-6249.

690   Shuhaimi-Othman M, Eng CL, Idris M (2007) Water Quality Changes in Chini Lake, Pahang, West
691   Malaysia. Environ. Monit. Assess. 131, 279–292.

692   Solovieva N, Jones VJ, Nazarova L, Brooks SJ, Birks HJB, Grytnes J-A, Appleby PG, Kauppila T,
693   Kondratenok BM, Renberg I, Ponomarev V (2005) Palaeolimnological evidence for recent
694   climatic change in lakes from the northern Urals, arctic Russia. J. Paleolimnol. 33, 463-482.

695   Stein AF, Draxler RR, Rolph GD, Stunder BJB, Cohen MD, Ngan F (2015) NOAA's HYSPLIT atmospheric
696   transport and dispersion modelling system. Bull. Amer. Meteor. Soc. 96, 2059-2077.

697   Stockholm International Water Institute (2009) *Securing water for ecosystem and human well-being:*
698   *the importance of environmental flows.* Swedish Water House Report 24. Stockholm,
699   Sweden.

700   Streets DG, Bond TC, Carmichael GR, Fernandes SD, Fu Q, He D, Klimont Z, Nelson SM, Tsai NY, Wang
701   MQ, Woo J-H, Yarber KF (2003) An inventory of gaseous and primary aerosol emissions in
702   Asia in the year 2000, J. Geophys. Res., 108, 8809.

703   Streets DG, Bond TC, Lee T, Jang C (2004) On the future of carbonaceous aerosol emissions. J.
704   Geophys. Res. 109, D24212.

705   Wang SX, Zhao B, Cai SY, Klimont Z, Nielsen CP, Morikawa T, Woo JH, Kim Y, Fu X, Xu JY, Hao JM, He
706   KB (2014) Emission trends and mitigation options for air pollutants in East Asia. Atmos.
707   Chem. Phys. 14, 6571–6603.

708   Wang ZH, Dong YH, Chen J, Li XF, Cao J, Deng ZY (2014). Dating recent sediments from the
709   subaqueous Yangtze Delta and adjacent continental shelf, China. J. Palaeogeog. 3, 207-218.

710   World Health Organisation Press (2016) *World health statistics 2016. Monitoring for the Sustainable*
711   *Development Goals.* Geneva, Switzerland.

712   Wu YH, Wang SM, Xia WL, Liu J (2005) Dating recent lake sediments using spheroidal carbonaceous
713   particle (SCP). Chin. Sci. Bull. 50, 1016-1020.

714   Yang H, Rose NL, Battarbee RW (2001) Dating of recent catchment peats using spheroidal
715   carbonaceous particle (SCP) concentration profiles with particular reference to Lochnagar,
716   Scotland. Holocene 11, 593-597.

717   Yang H, Berry A, Rose N, Berg T (2009) Decline in atmospheric mercury deposition in London. J.
718   Environ. Monit. 11, 1518-1522.

719   Yang, H, Battarbee, RW, Turner, SD, Rose, NL, Derwent, RG, Wu, G, Yang R (2010). Historical
720   reconstruction of mercury pollution across the Tibetan Plateau using lake sediments.
721   Environ. Sci. Technol. 44, 2918-2924.

722   Yang H, Turner S, Rose NL (2016) Mercury pollution in the lake sediments and catchment soils of
723   anthropogenically-disturbed sites across England. Environ. Pollut. 219, 1092-1101.

724 Yin J, Andersson H, Zhang S (2016) Air Pollution Control Policies in China: A Retrospective and

725 Prospects. Intern. J. Environ. Res. Publ. Health 13, 1219

726 Yoshikawa S, Yamaguchi S, Hata A (2000) Paleolimnological investigation of recent acidity changes in

727 Sawanoike Pond, Kyoto, Japan. J. Paleolimnol. 23, 285-304.

728 Zhao Y, Zhong H, Zhang J, Nielsen CP (2015) Evaluating the effects of China's pollution controls on

729 inter-annual trends and uncertainties of atmospheric mercury emissions. Atmos. Chem.

730 Phys. 15, 4317–4337.

731

732 **Figures**

733 Fig. 1: a-b) Map of sites and locations of power plants. SCL = Seven Crater Lakes (Philippines); TC =

734 Tasik Chini (Malaysia); SR = Singapore Reservoir (Singapore). Only power plants that started

735 operations prior to 2000 are shown for the Philippines; c-g) 3-day isobaric backward trajectories

736 ending at our study sites: Blue: air masses reaching the sites in the Philippines; green: air masses

737 reaching Tasik Chini (Malaysia); red: air masses reaching Singapore. Orange arrows summarise

738 seasonal wind directions based on the data shown in Supplementary Table 2, with panels showing

739 characteristic months that exemplify the seasonal (monsoonal) variability in wind directions in SEA.

740 Basemaps for (a) and (b) from www.freevectormaps.com

741

742 Fig. 2: Radiometric chronologies for the four dated records: Lake Mohicap, Lake Sampaloc, Lake

743 Yambo (all Philippines) and Tasik Chini (Malaysia) showing the CRS model ^{210}Pb dates and age (solid

744 lines) as well as the sedimentation rates (dashed lines)

745

746 Fig. 3: SCP concentrations for Lake Mohicap, Sampaloc and Yambo (Philippines), Lake Tasik Chini

747 (Malaysia) and a reservoir in Singapore (SR). Concentrations as number of particles per gram dry

748 material (n gDM^{-1})

749

750 Fig. 4: A. SCP fluxes for Lake Mohicap, Sampaloc and Yambo (Philippines) and Lake Tasik Chini

751 (Malaysia) expressed as numbers of particles per cm^2 per year (n cm^{-2} yr^{-1}). B. Coal (10^3 short tonnes;

752 ST) and oil (10^3 barrels/day; bd^{-1}) usage in selected SEA countries since 1980 (www.eia.gov) C.

753 Summary diagram for SEA with SCP sediment profile data from (a) normalized to the SCP

754 accumulation peak (1.0) for the individual sites. Open circles reflect individual data points; the red

755 line represents a general trend and is calculated by applying a LOESS smoother (span = 0.15) to the

756 data. Horizontal bar indicates 1950 ± 5 years representing the global increase in SCP contamination

757 during the mid-20th century (Rose 2015)

758

759   Fig. 5: SCP and Hg concentrations and fluxes for (a) Lake Sampaloc and (b) Lake Yambo (Philippines).

760   Concentration curves on a depth (cm) scale; fluxes on an age scale with a secondary depth scale
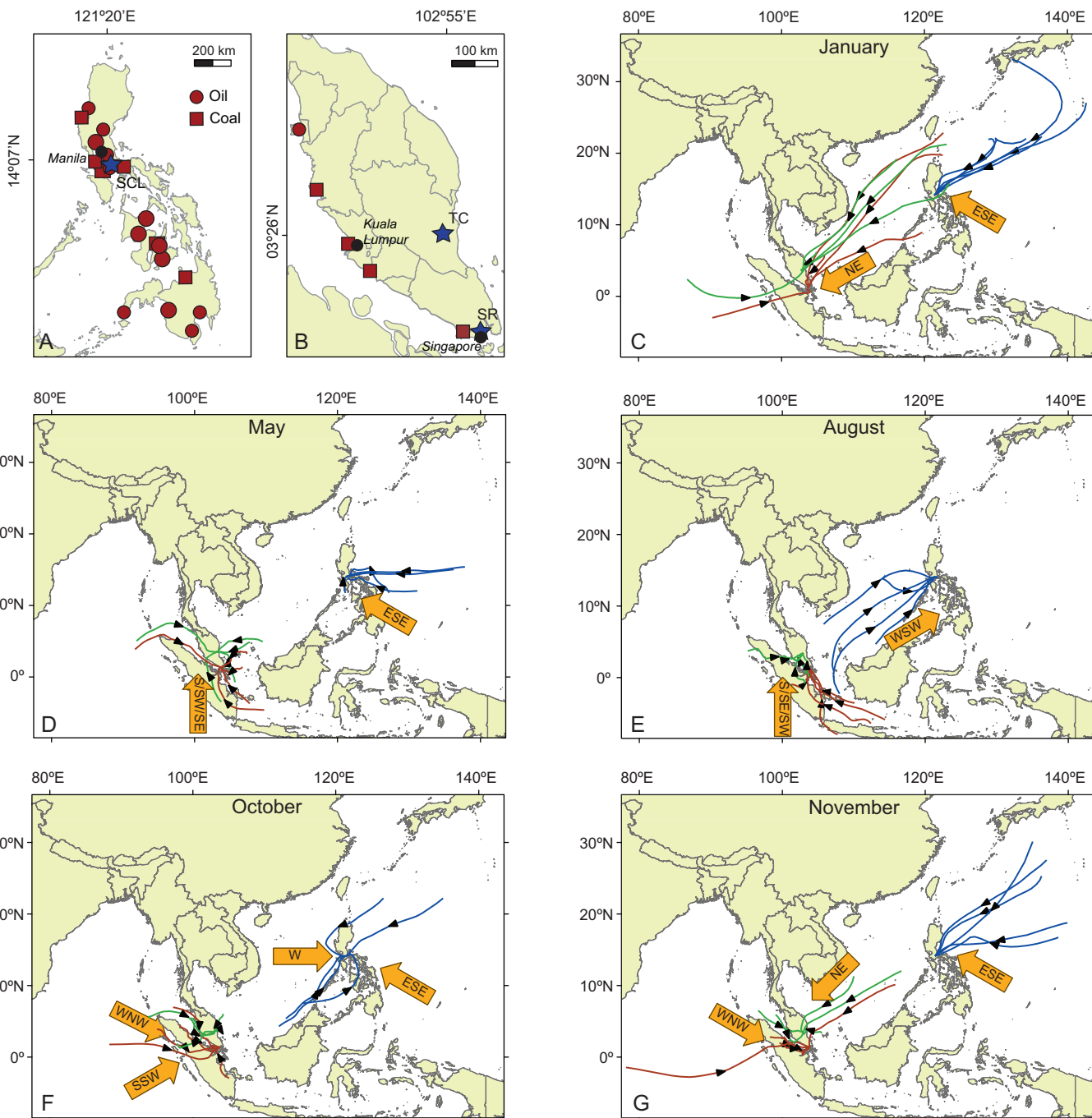
761   plotted for comparison

Figure 1

Fig. 1: a-b) Map of sites and locations of power plants. SCL = Seven Crater Lakes (Philippines); TC = Tasik Chini (Malaysia); SR = Singapore Reservoir (Singapore). Only power plants that started operations prior to 2000 are shown for the Philippines; c-g) 3-day isobaric backward trajectories ending at our study sites: Blue: air masses reaching the sites in the Philippines; green: air masses reaching Tasik Chini (Malaysia); red: air masses reaching Singapore. Orange arrows summarise seasonal wind directions based on the data shown in Supplementary Table 2, with panels showing characteristic months that exemplify the seasonal (monsoonal) variability in wind directions in SEA. Basemaps for (a) and (b) from www.freevectormaps.com
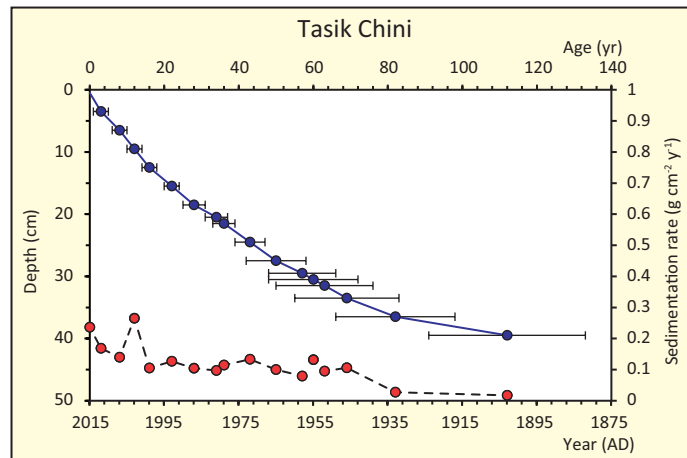
Figure 2
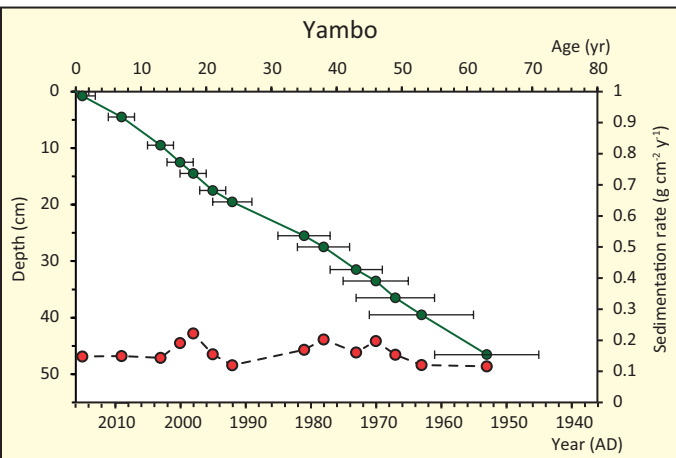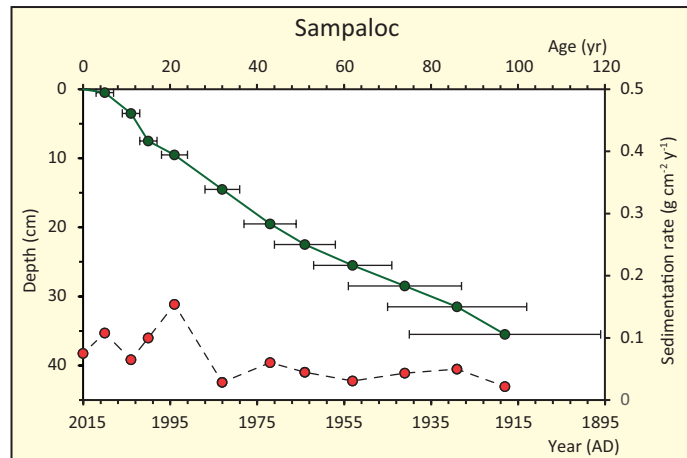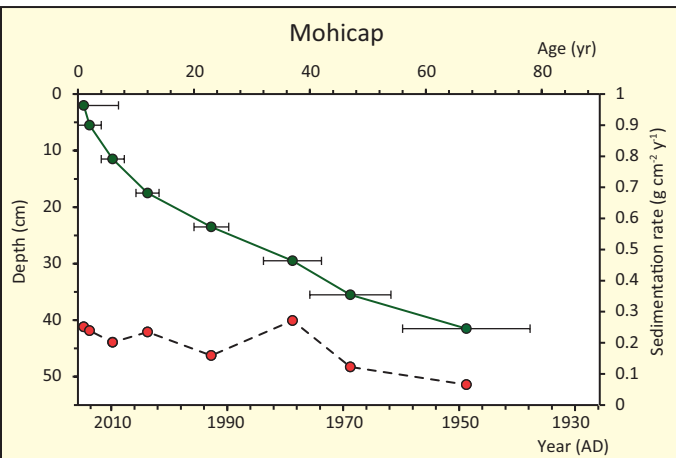
Fig. 2: Radiometric chronologies for the four dated record: Lake Mohicap, Lake Sampaloc, Lake Yambo (all Philippines) and Tasik Chini (Malaysia) showing the CRS model ^{210}Pb dates and age (solid lines) as well as the sedimentation rates (dashed lines)

Figure 3
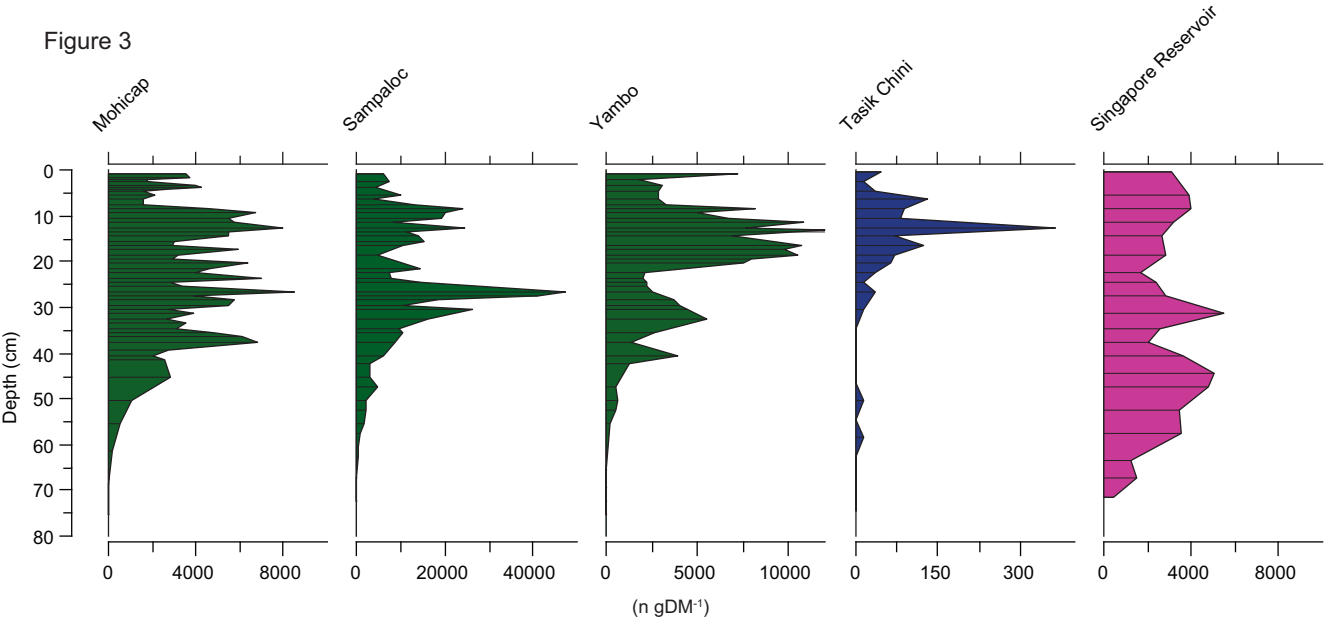
Fig. 3: SCP concentrations for Lake Mohicap, Sampaloc and Yambo (Philippines), Lake Tasik Chini (Malaysia) and a reservoir in Singapore (SR). Concentrations as number of particles per gram dry material (n gDM⁻¹)
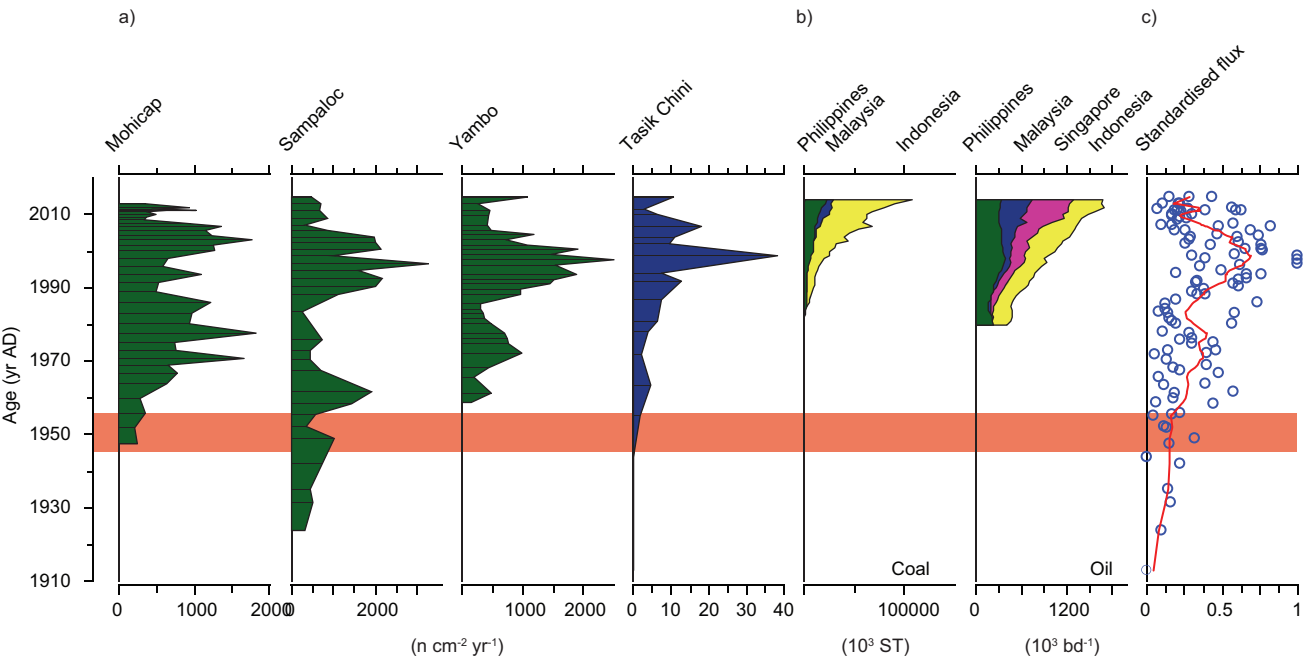
Fig. 4: A. SCP fluxes for Lake Mohicap, Sampaloc and Yambo (Philippines) and Lake Tasik Chini (Malaysia) expressed as numbers of particles per cm² per year (n cm⁻² yr⁻¹). B. Coal (10³ short tonnes; ST) and oil (10³ barrels/day; bd⁻¹) usage in selected SEA countries since 1980 (www.eia.gov) C. Summary diagram for SEA with SCP sediment profile data from (a) normalized to the SCP accumulation peak (1.0) for the individual sites. Open circles reflect individual data points; the red line represents a general trend and is calculated by applying a LOESS smoother (span = 0.15) to the data. Horizontal bar indicates 1950 ± 5 years representing the global increase in SCP contamination during the mid-20th century (Rose 2015)

Fig. 5: SCP and Hg concentrations and fluxes for (a) Lake Sampaloc and (b) Lake Yambo (Philippines). Concentration curves on a depth (cm) scale; fluxes on an age scale with a secondary depth-scale plotted for comparison

Supplementary information

Table S1: Site information. Surface area is an approximation as this will seasonally vary for some of the sites. Water depths as recorded at time of coring.

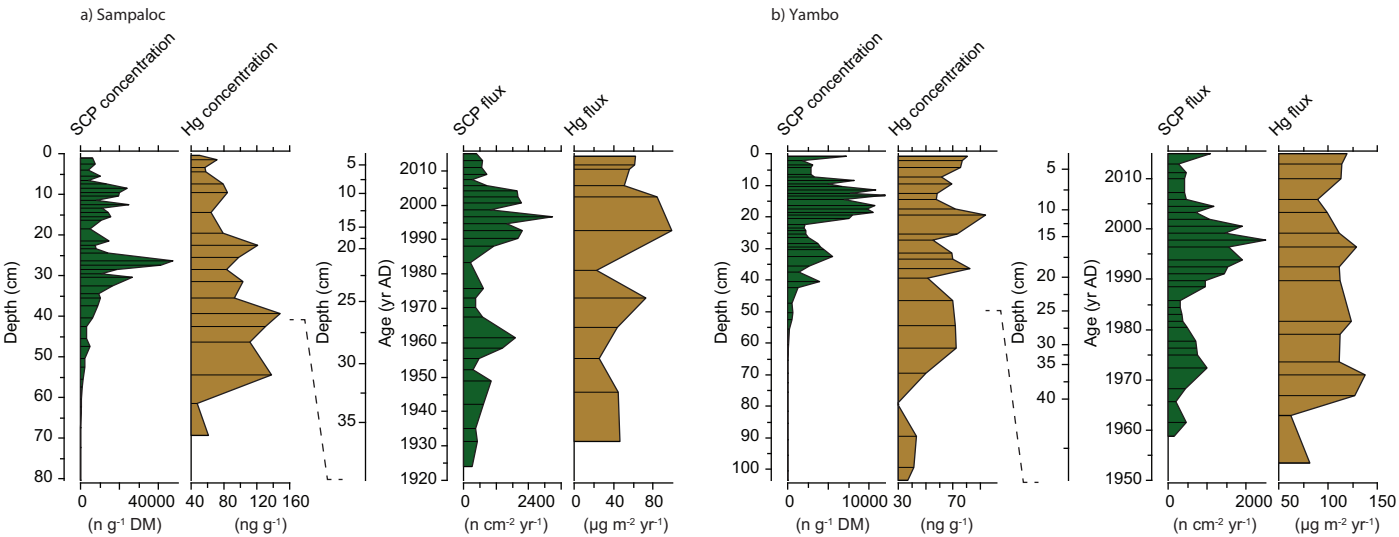| Site	Latitude (N)	Longitude (E)	Altitude (m)	Surface area (km^2)	Water depth (m)	Lake type	Length obtained core (cm)
Philippines							
Mohicap	14°07'19"	121°20'03"	99	0.23[a]	30.4	Crater lake	87
Sampaloc	14°04'44"	121°19'47"	108	1.04[a]	27.6	Crater lake	81
Yambo	14°07'09"	121°21'59"	207	0.30[a]	38.0	Crater lake	104
Malaysia							
Tasik Chini	03°26'01"	102°55'43.1"	12	2.0[b]	2.5	Floodpulse wetland	75
Singapore							
Reservoir	01°22'13"	103° 48'11"	42	3.2[c]	7.8	Reservoir	72

a) Brillo BBC (2016) Developing Mohicap Lake, San Pablo City, Philippines. Soc. Sci. 11, 283-290.
b) Shuhaimi-Othman M, Eng CL, Idris M (2007) Water Quality Changes in Chini Lake, Pahang, West Malaysia. Environ. Monit. Assess. 131, 279–292.
c) Public Utilities Board Website; http://www.pub.gov.sg/abcwatersIM/upper-peirce.html

Table S2: Monthly measurements of wind directions and precipitation amounts for each of our study areas. Color codes in table 2a indicate time intervals with similar wind conditions. Black boxes indicate months selected for backward trajectory modelling

Table S2a. Monthly wind patterns

	Jan	Feb	Mar	Apr	May	Jun	Jul	Aug	Sep	Oct	Nov	Dec
Philippines	ESE	ESE	ESE	ESE	WSW-ESE	WSW-ESE	WSW-ESE	WSW	WSW	WSW-ESE	ESE	ESE
Malaysia	SW-NE	SW-NE	SW-NE	SW-NE	SSE	SSE	SSE	SSE	SSE	WNW-SSW	WNW-NNE	NW-NE
Singapore	NE	NE	NE	NE	SSW	SSW	SSW	SSW	SSW	SSW	NE	NE

Wind directions retrieved from the freely available data on:
https://www.windfinder.com/windstatistics/manila_airport
https://www.windfinder.com/windstatistics/morib_kuala_lumpur
https://www.windfinder.com/windstatistics/singapore_changi

Table S2b. Monthly precipitation (mm)

	Jan	Feb	mar	Apr	May	Jun	Jul	Aug	Sep	Oct	Nov	Dec
Philippines	5	34	10	23	126	101	274	648	96	251	44	66
Malaysia	115	110	154	254	427	235	315	149	174	169	629	290
Singapore	293	231	177	260	174	115	137	123	124	228	378	409

Philippines: measurements for Manila, year: 2016; data from www.worldweatheronline.com
Malaysia: measurements for Kuala Lumpur, year: 2016; data from www.worldweatheronline.com
Singapore: measurements for Singapore City, year: 2016; data from www.worldweatheronline.com

Table S3a. ^{210}Pb and ^{137}Cs concentrations in core MOH taken from Mohicap, Philippines.

| Depth | Dry Mass | Pb-210 | | | | | | Cs-137 | |
| | | Total | | Supported | | Unsupp | | | |
cm	g cm^{-2}	Bq Kg^{-1}	±	Bq Kg^{-1}	±	Bq Kg^{-1}	±	Bq Kg^{-1}	±
2.0	0.1907	186.45	25.77	41.13	7.19	145.32	26.75	0	0
5.5	0.5337	175.01	20.89	28.81	5.66	146.20	21.64	0	0
11.5	1.3437	191.27	21.59	36.55	6.01	154.72	22.41	0	0
17.5	2.6547	147.99	16.05	37.85	4.40	110.17	16.64	0	0
23.5	4.8498	130.70	15.00	16.56	3.75	114.14	15.46	0	0
29.5	7.6704	75.04	7.55	31.72	2.04	43.32	7.82	0	0
35.5	9.5238	98.93	13.53	29.01	3.68	69.92	14.02	3.31	1.68
41.5	11.2548	101.49	10.56	29.24	2.69	72.25	10.90	0	0
47.5	15.9975	33.67	11.68	38.63	3.69	-4.96	12.25	0	0
54.5	23.5701	59.87	18.72	36.92	2.46	-7.05	18.88	0	0
61.5	29.5457	42.00	23.36	52.03	6.03	-10.03	24.13	0	0

Table S3b. ^{210}Pb and ^{137}Cs concentrations in core SAMP taken from Sampaloc, Philippines.

| Depth | Dry Mass | Pb-210 | | | | | | Cs-137 | |
| | | Total | | Supported | | Unsupp | | | |
cm	g cm^{-2}	Bq Kg^{-1}	±	Bq Kg^{-1}	±	Bq Kg^{-1}	±	Bq Kg^{-1}	±
0.5	0.031	189.61	18.76	25.84	3.89	163.77	19.16	0	0
3.5	0.4713	125.17	14.04	27.33	3.37	97.84	14.44	0	0
7.5	0.9571	161.75	13.73	26.41	3.24	135.34	14.11	0	0
9.5	1.2822	118.42	26.54	40.84	6.16	77.58	27.25	0	0
14.5	1.991	85.44	13.66	43.36	3.02	42.08	13.99	0	0
19.5	2.6652	212.88	33.03	51.12	7.85	161.76	33.95	0	0
22.5	3.0848	86.63	13.83	31.69	3.62	54.94	14.3	0	0
25.5	3.5043	112.18	25.03	54.37	6.42	57.81	25.84	0	0
28.5	3.9305	92.49	13.38	33.4	4.36	59.09	14.07	0	0
31.5	4.3566	66.32	13.75	37.64	4.63	28.68	14.51	0	0
35.5	4.9398	41.12	9.37	31.3	3.21	9.82	9.9	0	0
39.5	5.523	61.48	9.88	33.56	3.21	27.92	10.39	0	0
42.5	6.0576	55.44	7.79	30.8	2.47	24.64	8.17	0	0
46.5	6.7704	38.22	9.15	46.47	2.47	-8.25	9.48	0	0
54.5	8.4348	38.22	9.86	38.83	2.48	-0.61	10.17	0	0
69.5	11.7134	25.03	7.75	31.78	2.32	-6.75	8.09	0	0

Table S3c. ^{210}Pb and ^{137}Cs concentrations in core YAMB taken from Yambo, Philippines.

| Depth | Dry Mass | Pb-210 | | | | | | Cs-137 | |
| | | Total | | Supported | | Unsupp | | | |
cm	g cm^{-2}	Bq Kg^{-1}	±	Bq Kg^{-1}	±	Bq Kg^{-1}	±	Bq Kg^{-1}	±
0.75	0.1188	210.23	17.38	44.97	4.19	165.26	17.88	0	0
4.5	1.0329	173.6	13.81	38.15	3.17	135.45	14.17	4.29	1.33
9.5	1.9378	159.12	18.7	43.17	4.14	115.95	19.15	0	0
12.5	2.446	115.47	12.66	36.25	3.18	79.22	13.05	0	0
14.5	2.7848	102.58	12.45	37.75	3.39	64.83	12.9	0	0
17.5	3.341	112.62	13	28.15	2.98	84.47	13.34	0	0
19.5	3.7118	149.55	13.55	48.8	3.7	100.75	14.05	0	0
25.5	5.2979	94.3	8.33	44.43	2.13	49.87	8.6	5.21	0.79
27.5	5.8124	73.8	10.19	35.54	2.75	38.26	10.55	0	0
31.5	6.8414	78.78	11.31	38.36	3.21	40.42	11.76	6.43	1.47
33.5	7.2229	62.26	6.77	31.53	1.78	30.73	7	6.34	0.85

Depth	Dry Mass	Pb-210 Total	±	Supported	±	Unsupp	±	Cs-137	±
36.5	7.7952	81	11.4	45.26	2.99	35.74	11.79	6.12	1.4
39.5	8.3674	81.38	8.27	41.49	2.18	39.89	8.55	15.94	1.23
46.5	9.507	69.45	10.09	38.75	2.81	30.7	10.47	0	0
54.5	10.787	27.21	6.82	39.71	2.03	-12.5	7.12	1.53	0.82
61.5	12.0589	42.3	8.39	43.69	2.97	-1.39	8.9	2.86	1.37
69.5	13.3613	48.04	7.33	36.11	2.57	11.93	7.77	0	0
79.5	16.7343	27.91	4.81	34.25	1.59	-6.34	5.07	0	0

Table S3d. ^{210}Pb and ^{137}Cs concentrations in core TC-1a taken from Tasik Chini, Malaysia

Depth	Dry Mass	Pb-210 Total		Supported		Unsupp		Cs-137	
cm	g cm^{-2}	Bq Kg^{-1}	±	Bq Kg^{-1}	±	Bq Kg^{-1}	±	Bq Kg^{-1}	±
0.5	0.0629	222.37	18.68	99.3	6.6	123.07	19.81	0	0
3.5	0.5566	261.24	25.25	101.91	6.87	159.33	26.17	0	0
6.5	1.3096	258.91	15.12	93.59	4.21	165.32	15.7	0	0
9.5	2.0703	180.6	12.69	103.94	4.13	76.66	13.35	0	0
12.5	2.831	289.54	17.23	121.56	5.16	167.98	17.99	0	0
15.5	3.4948	243.46	14.61	127.83	4.59	115.63	15.31	0	0
18.5	4.1993	246.71	8.2	130.11	2.51	116.6	8.58	1.70	0.93
20.5	4.727	231.31	14.74	125.17	4.66	106.14	15.46	0	0
21.5	4.9952	222.06	13.18	138.56	4.66	83.5	13.98	3.21	1.61
24.5	5.8104	207.79	14.69	149.46	4.85	58.33	15.47	0	0
27.5	6.6602	208.11	14.27	146.57	4.81	61.54	15.06	0	0
29.5	7.242	193.97	12.92	130.19	4.32	63.78	13.62	0	0
30.5	7.5406	168	8.22	133.3	2.64	34.7	8.63	0	0
31.5	7.867	175.94	12.34	131.88	4.09	44.06	13	0	0
33.5	8.47	163.96	12.98	131.15	4.36	32.81	13.69	0	0
36.5	9.1938	229.49	18.23	147.58	5.82	81.91	19.14	0	0
39.5	9.8468	204.35	10.35	151.23	3.57	53.12	10.95	0	0
42.5	10.4958	169.54	13.99	147.42	4.96	22.12	14.84	0	0
45.5	11.174	139.73	12.95	143.78	4.8	-4.05	13.81	0	0
48.5	11.8296	147.14	16.61	143.79	4.74	3.35	17.27	0	0

Figure S1a: Typical plot of variations over time in altitude of air parcels arriving at three study sites: January 1st 2017
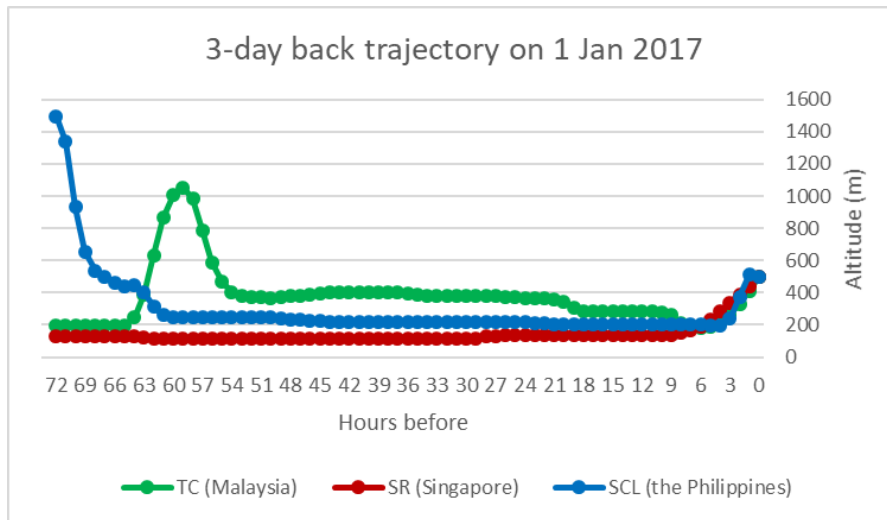

Figure S1b: Typical plot of variations over time in altitude of air parcels arriving at three study sites: May 1st 2016
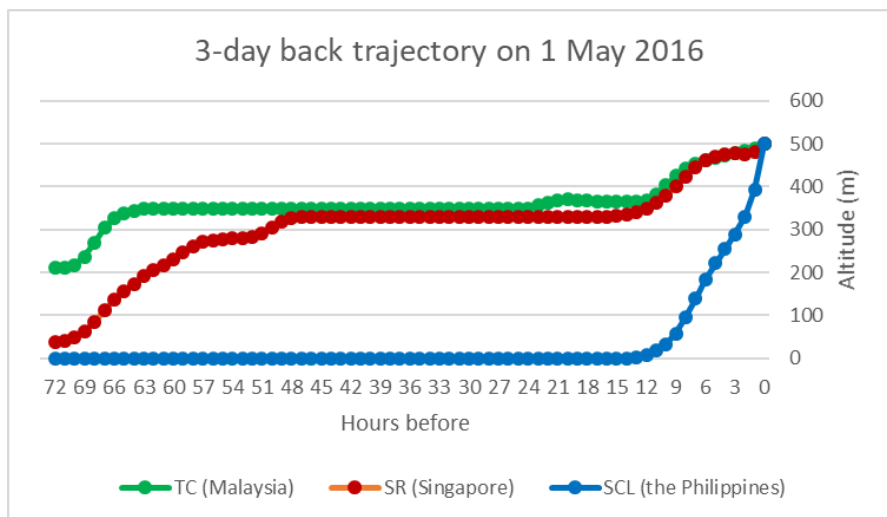

Figure S1c: Typical plot of variations over time in altitude of air parcels arriving at three study sites: August 1st 2016
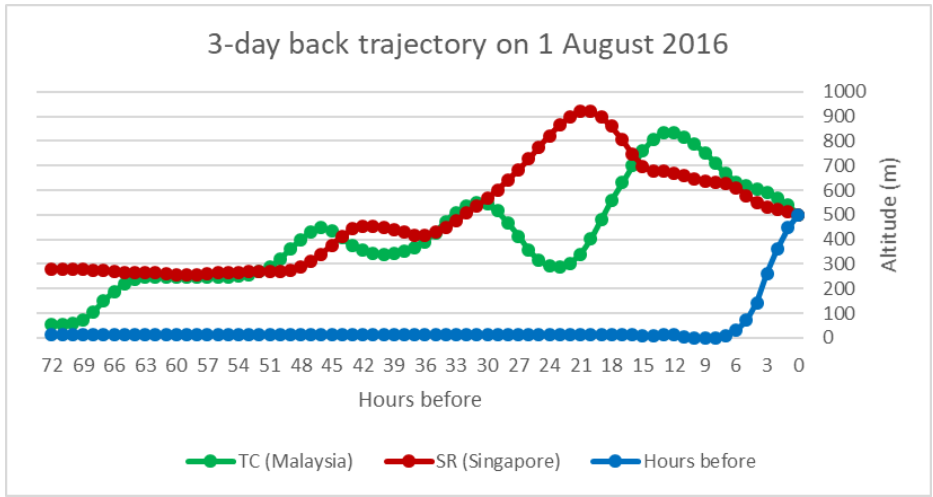
3-day back trajectory on 1 August 2016

Figure S1d: Typical plot of variations over time in altitude of air parcels arriving at three study sites: October 1st 2016
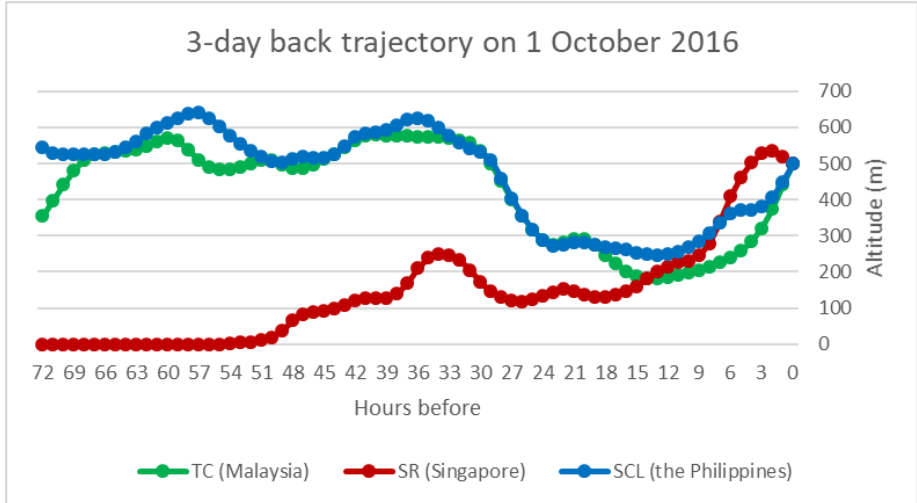

3-day back trajectory on 1 October 2016

Figure S1e: Typical plot of variations over time in altitude of air parcels arriving at three study sites: November 1st 2016

3-day back trajectory on 1 November 2016